Citation: Molecular Therapy—Nucleic Acids (2016) 5, e397; doi:10.1038/mtna.2016.102
Official journal of the American Society of Gene & Cell Therapy
www.nature.com/mtna

A Novel PD-L1-targeting Antagonistic DNA Aptamer With Antitumor Effects

Wei-Yun Lai[1,2], Bo-Tsang Huang[2], Jen-Wei Wang[1,2], Pei-Ying Lin[2,3] and Pan-Chyr Yang[2,4]

The PD-1/PD-L1 axis is a major pathway involved in tumor immune evasion. Here, we report the novel PD-L1 antagonizing DNA aptamer (aptPD-L1) and demonstrate an integrated pipeline that expedites therapeutic aptamer development. Aptamer can exert antibody-mimic functions and is advantageous over antibody for its chemically synthetic nature, low immunogenicity, and efficient tissue penetration. Our results showed that aptPD-L1 blocked the binding between human PD-1 and PD-L1. Experiments using murine models showed that aptPD-L1 promoted *in vitro* lymphocyte proliferation and suppressed *in vivo* tumor growth without the induction of observable liver or renal toxicity. Analyses on the aptPD-L1-treated tumors further revealed elevated levels of infiltrating $CD4^+$ and $CD8^+$ T cells, intratumoral IL-2, TNF-α, interferon (IFN)-γ and the C-X-C motif chemokines, CXCL9 and CXCL10. The $CD8^+$ T cells in the aptPD-L1-treated tumors had higher CXCR3 expression level compared to the random-sequence oligonucleotides-treated ones. Besides, the length and density of $CD31^+$ intratumoral microvessels were significantly decreased in the aptPD-L1 treatment group. Collectively, our data suggested that aptPD-L1 helps T cell function restoration and modifies tumor microenvironment. These chemokines might orchestrate together to attract more T cells into the tumor tissues to form the positive amplification loop against tumor growth, indicating the translational potential of aptPD-L1 in cancer immunotherapy.

Molecular Therapy—Nucleic Acids (2016) **5**, e397; doi:10.1038/mtna.2016.102; published online 13 December 2016
Subject Category: Aptamers, ribozymes and DNAzymes

Introduction

Immune checkpoint blockade has opened a new era for cancer therapy. Accumulating evidences indicate that monoclonal antibodies targeting CTLA-4, PD-1, or PD-L1 exert durable clinical response in many treatment-refractory cancers.[1–5] PD-1 is a coinhibitory molecule of T cell receptor signaling expressed on activated T cells.[6] Its ligand, PD-L1, is expressed in both cancer cells and tumor-infiltrating lymphocytes.[7] The engagement of PD-1/PD-L1 suppresses T cell function and the axis is considered one of the major pathways involved in tumor immune evasion.[8] Here we report the novel PD-L1 antagonistic DNA aptamer, aptPD-L1, which exhibits tumor inhibitory functions. Taking the advantage of aptamer, aptPD-L1 may work as a complementary therapeutics.[9,10]

Aptamer has long been considered as an antibody surrogate due to its capability of forming complex three-dimensional (3D) structures, high specific binding affinity, and low immunogenicity.[11–13] Aptamer is relatively small in size (6–30 kDa) and possesses better tissue penetration efficiency. It is chemically synthesized and is structurally easy to be modified. Aptamer can therefore be synthesized in large scale with controllable batch-to-batch variations and be customized modified for specific therapeutic applications with different formulations.[14–16] Aside from systemic delivery through intravenous administration, aptamer can be coupled to various materials for controlled and sustained release at restricted areas, such as eye, vagina, joint, and lung.[17–20]

Traditional aptamer selection process is time-consuming. It takes repetitive rounds of partition and amplification for specific aptamer clusters enrichment.[21,22] Individual sequence is then obtained by Sanger sequencing, followed by affinity assessment. The tedious process prohibits high-throughput aptamer identification and high-affinity does not always translate to biological effectiveness. These are the canonical pitfalls in therapeutic aptamer development. In the current study, we demonstrated the developmental pipeline of aptPD-L1. The efficient pipeline integrated five technical platforms, including systematic evolution of ligands by exponential enrichment (SELEX), next-generation sequencing (NGS), sequence alignment algorithms and structural prediction software, quantitative polymerase chain reaction (qPCR), and enzyme-linked immunosorbent assay (ELISA)-based competition platform. Our results showed that aptPD-L1 specifically binds to human and mouse PD-L1 proteins, leading to PD-1/PD-L1 axis inhibition and T cell function restoration (**Figure 1**). The data suggest the potential of aptPD-L1 to be developed into a new therapeutic agent in human cancer immunotherapy.

Results

Human PD-L1-targeting aptamers were identified using a nitrocellulose filter SELEX (**Figure 2a**). By adopting NGS platform, the SELEX round was reduced from 15 or above to 8 in the current study. ssDNAs with more than 160 output

The last two authors contributed equally to this work.
[1]Aptamer Core Facility, Institute of Biomedical Sciences, Academia Sinica, Taipei, Taiwan; [2]Institute of Biomedical Sciences, Academia Sinica, Taipei, Taiwan; [3]National Center of Excellence for Clinical Trials and Research Center, Department of Medical Research, National Taiwan University Hospital, Taipei, Taiwan; [4]Department of Internal Medicine, National Taiwan University Hospital and College of Medicine, Taipei, Taiwan. Correspondence: Pan-Chyr Yang, President, National Taiwan University, Professor of Internal Medicine, National Taiwan University College of Medicine, No. 1, Sec. 4, Roosevelt Rd., Taipei 1061, Taiwan. E-mail: pcyang@ntu.edu.tw
Keywords: aptamer; immunotherapy; PD-1; PD-L1; tumor microenvironment
Received 22 June 2016; accepted 21 October 2016; published online 13 December 2016. doi:10.1038/mtna.2016.102

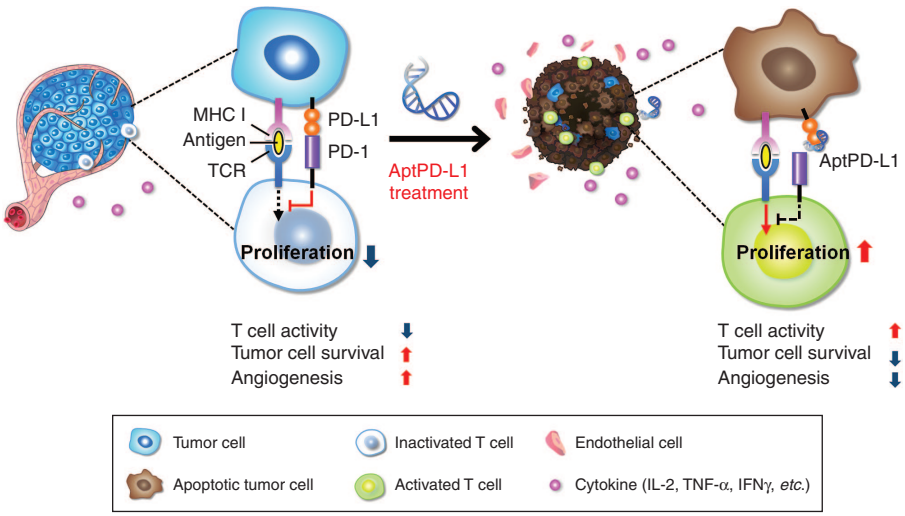

Figure 1 AptPD-L1 blocks PD-1/PD-L1 interaction and attenuates T cell suppression. The induced expression of cytokines (IL-2, TNF-α, IFNγ, CXCL9, and CXCL10) collectively contributes to the suppression effects on intratumoral microvessel formation and tumor cell survival.

reads (87.32% of total output reads, **Supplementary Table S1**) were analyzed by sequence alignment algorithms, Clustal Omega and FASTAptamer, and categorized into groups.[23,24] The binding affinity of the candidate aptamers and their truncated relatives was evaluated using a 96-well formatted nitrocellulose filter binding assay combined with 384-well formatted quantitative PCR. For those with affinity < 10 nmol/l, their potencies for PD-L1/PD-1 blockade were examined using PD-L1 ELISA-based competition platform (**Supplementary Figure S1a**). The results showed that the 45-nucleotide-long aptPD-L1 specifically bound to human PD-L1 with a dissociation constant (Kd) of 4.7 nmol/l rather than nonrelevant protein bovine serum albumin and blocked 58% of the interaction between PD-1 and PD-L1 (**Figure 2b**). Secondary structures predicted by Mfold revealed that aptPD-L1 has a long-stem structure formed by the 5' and 3' ends, and two short-stem loops formed by the remaining sequences (**Figure 2c**, left panel). 3D-strucure prediction and docking simulation (**Figure 2c**, right panel) further suggested that the short-stem loop located at the nucleotides 25–35 of aptPD-L1 blocks the binding between PD-L1 and PD-1[25] (**Supplementary Figure S1b**). The long-stem structure, on the other hand, interacts with the other domain of the PD-L1 protein and stabilizes the aptamer/protein complex. We next investigated whether aptPD-L1 binds to PD-L1 proteins expressed on human cells. PD-L1-low and PD-L1-high human cancer cell lines, A549 and HOP92, were incubated with fluorescence-labeled aptPD-L1. In consistent with endogenous PD-L1 protein levels, the fluorescence intensity was stronger in HOP92 cells than in A549 cells (**Figure 2d**). The data indicated that aptPD-L1 does bind to human PD-L1 protein expressed on cell surface.

The amino acid sequences of human and murine PD-L1 proteins are 77% identical.[25] Given that functional studies of immune checkpoint inhibitors are typically carried out in murine syngeneic tumor models, we examined if aptPD-L1 recognized murine PD-L1 protein. The nitrocellulose binding assay showed that aptPD-L1 bound to recombinant murine PD-L1 protein with a K_d of 72 nmol/l (**Figure 3a**). The result was supported by the flow cytometry analyses, which showed that aptPD-L1 bound to PD-L1 proteins expressed on CT26 and LL/2 cells (**Supplementary Figure S2a,b**). Immunofluorescence staining further revealed that aptPD-L1 stained the murine lymphocytes in a pattern similar to that of an anti-murine PD-L1 antibody. The mean thresholded Manders colocalization coefficients were 0.77 and 0.85 for aptPD-L1 and anti-murine PD-L1 antibody, respectively (**Figure 3b**). We then evaluated whether aptPD-L1 antagonizes immunosuppressive effects mediated by the PD-1/PD-L1 axis. Lymphocytes purified from BALB/c mice were labeled with CFSE, cocultured with unlabeled irradiated allogenic antigen-presenting cells, and treated with aptPD-L1 or random-sequence oligonucleotides. As shown in **Figure 3c**, 50% of CFSE-labeled lymphocytes underwent proliferation in the aptPD-L1-treated group, an increase of 10 percentage points compared to the random-sequence-treated group (40%). Similar results were also obtained in lymphocytes isolated from C57BL/6 mice, where aptPD-L1 treatment enhanced lymphocyte proliferation by 56% compared with 46% in the random-sequence-treated group (**Figure 3d**). The data suggested that aptPD-L1 is biologically active and can be functionally investigated in murine models.

CT26 and LL/2 murine syngeneic tumor models were adopted in the study of aptPD-L1 *in vivo* tumor inhibitory function. The data showed that successive doses of intraperitoneally aptPD-L1 administration (1.2 mg/kg) led to significant tumor-suppressive effect in both CT26-inoculated BALB/c mice (**Figure 4a**) and LL/2-inoculated C57BL/6 mice (**Figure 4b**). The tumor suppressive effect of aptPD-L1 was similar to that of anti-murine PD-L1 antibody (10 mg/kg). *In vitro* cell viability assay was further carried out to exclude direct cytotoxicity of aptPD-L1 against CT26 and LL/2 cells. The results showed that aptPD-L1 has no direct cytotoxicity on cancer cells (**Supplementary Figure S3**). Body weight measurement and blood biochemical analyses on liver and renal functions did not reveal significant differences in

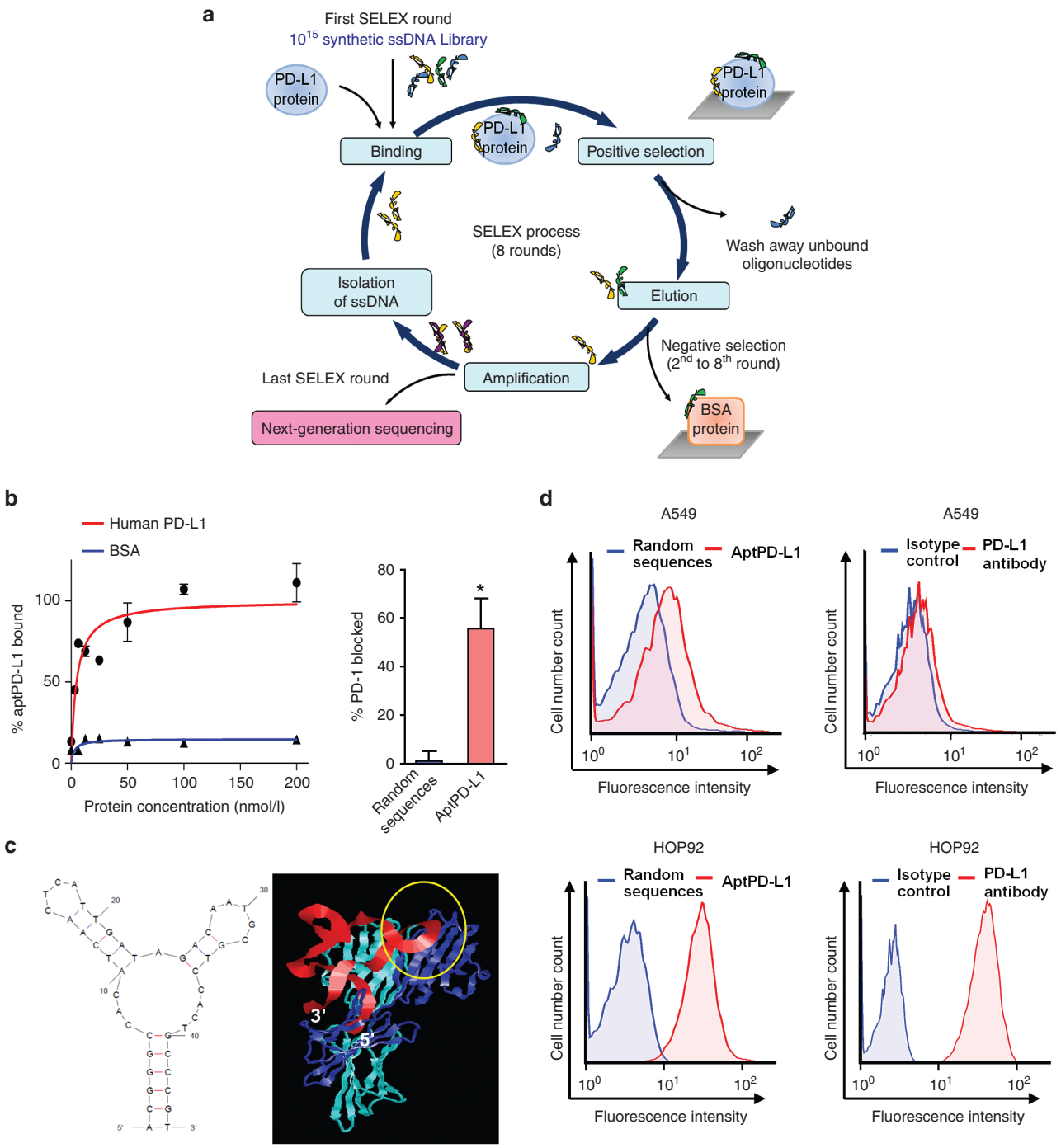

Figure 2 AptPD-L1 blocks PD-L1/PD-1 interactions. (**a**) Schematic illustration of Nitrocellulose filter SELEX. (**b**) The dissociation constant and antagonistic function of aptPD-L1 was determined using a nitrocellulose filter binding assay ($n = 3$) and an enzyme-linked immunosorbent assay-based competition assay (200 nmol/l, $n = 3$). (**c**) The predicted secondary structure of aptPD-L1 and docking simulation of aptPD-L1 (red) with PD-L1 protein (blue). The yellowish circle represents the binding region between PD-L1 and PD-1. (**d**) AptPD-L1 bound to A549 and HOP92 human cancer cells. The data are presented as mean ± standard error of the mean and were analyzed by Student's *t*-test. Asterisks denote statistical significant differences ($P < 0.05$).

the buffer-treated, the random-sequence oligonucleotides-treated, or the aptPD-L1-treated groups (**Supplementary Figure S4** and **Supplementary Table S2**). The results indicated that while being effective as an antitumor agent, aptPD-L1 does not bring up observable toxicity in murine models.

We further evaluated the biodistribution of aptPD-L1. Fluorescence-labeled aptPD-L1 was intraperitoneally administrated to the mice that bore PD-L1-expressing CT26 tumors. The results showed that while a significant increase in fluorescent signal emission was detected in the tumor tissue

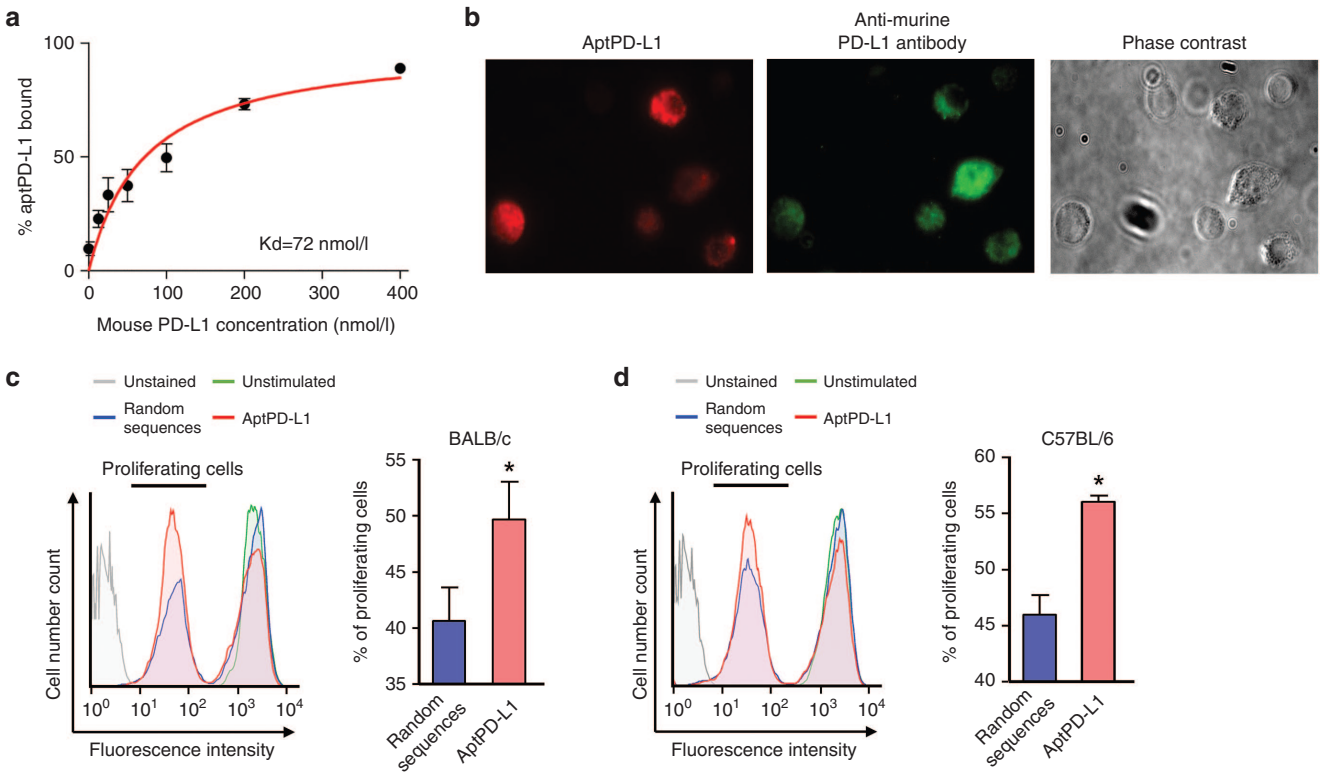

Figure 3 AptPD-L1 binds to PD-L1-expressing mouse lymphocytes and induces lymphocyte proliferation. (**a**) The dissociation constant of aptPD-L1 toward mouse PD-L1 was determined using a nitrocellulose filter binding assay ($n = 3$). (**b**) Mouse lymphocytes were simultaneously stained with aptPD-L1 (red) and an anti-murine PD-L1 antibody (green). (**c, d**) The proliferation status of CFSE-labeled mouse lymphocytes after a 72-hour treatment with random-sequence oligonucleotides or aptPD-L1 (200 nmol/l, $n = 3$). The data are presented as mean ± standard error of the mean and were analyzed by Student's *t*-test. Asterisks denote statistical significant differences ($P < 0.05$).

obtained from the aptPD-L1-treated mice, fluorescent signal was mainly detected in the kidney in the random-sequence oligonucleotides-treated group (**Figure 4c**). The results suggested that aptPD-L1 accumulated in the PD-L1-expressing CT26 tumor tissues where it might interrupt the interaction between PD-L1 and PD-1.

Analyses of responders to Atezolizumab (Roche), an anti-PD-L1 antibody, revealed increased *TNF-α*, *IFNγ* and chemokine *CXCL9/10* levels in the post-treatment tumors.[5] We therefore examined whether similar phenomena were observed in the aptPD-L1-treated CT26 and LL/2 tumors. Consistent with these previous findings, the immunoblot analyses showed elevated IL-2, TNF-α, and IFNγ in the aptPD-L1-treated tumors (**Figure 5a**). Moreover, the expression of IFNγ-inducible chemokines CXCL9 and CXCL10 were increased in the aptPD-L1-treated tumors by qPCR and immunoblot analyses (**Figure 5b** and **Supplementary Figure S5**).

Intratumoral CXCL9/10 has been reported to exert antitumor effects.[26–28] We first evaluated the correlation between chemokine levels and the size of tumors. The results revealed that levels of CXCL9 and CXCL10 were negatively correlated with tumor size (Pearson $r = –0.45$ and –0.49, respectively). We next investigated whether the aptPD-L1-treated tumors had higher levels of T cell infiltration compared to the random-sequence oligonucleotides-treated ones. Both flow cytometry and immunohistochemistry staining analyses showed significantly increased $CD4^+$ and $CD8^+$ T cells in the aptPD-L1-treated tumors (**Figure 5c**,**d**). In addition, the infiltrating $CD8^+$ T cells within these tumors had higher CXCR3 expression than the random-sequence oligonucleotides-treated ones (**Figure 5e**). The chemokines CXCL9/10 are also known to inhibit angiogenesis through their binding to endothelial cells.[26] We thus investigated the effects of aptPD-L1 treatment on intratumoral microvessels. Our results showed that both the length and density of $CD31^+$ intratumoral microvessels were significantly decreased in the aptPD-L1 treatment group (**Figure 5f**). Collectively, our data demonstrated the antitumor activity of aptPD-L1. AptPD-L1 helps T cell function restoration, modulates tumor microenvironment, and possibly forms the positive amplification loop against tumor growth.The results suggested a translational potential of aptPD-L1 as an alternative therapeutics to anti-PD-L1 antibody.

Discussion

In the current study, we reported the first PD-L1 antagonistic DNA aptamer with translational potential and demonstrated an efficient pipeline for therapeutic aptamer development. The pipeline integrated five technical platforms. The SELEX enriched the target-specific ssDNA sequences. The NGS data computation and sequence alignment provided a broader spectrum of sequence information. With the combination of qPCR and ELISA platforms, we retrieved aptamers

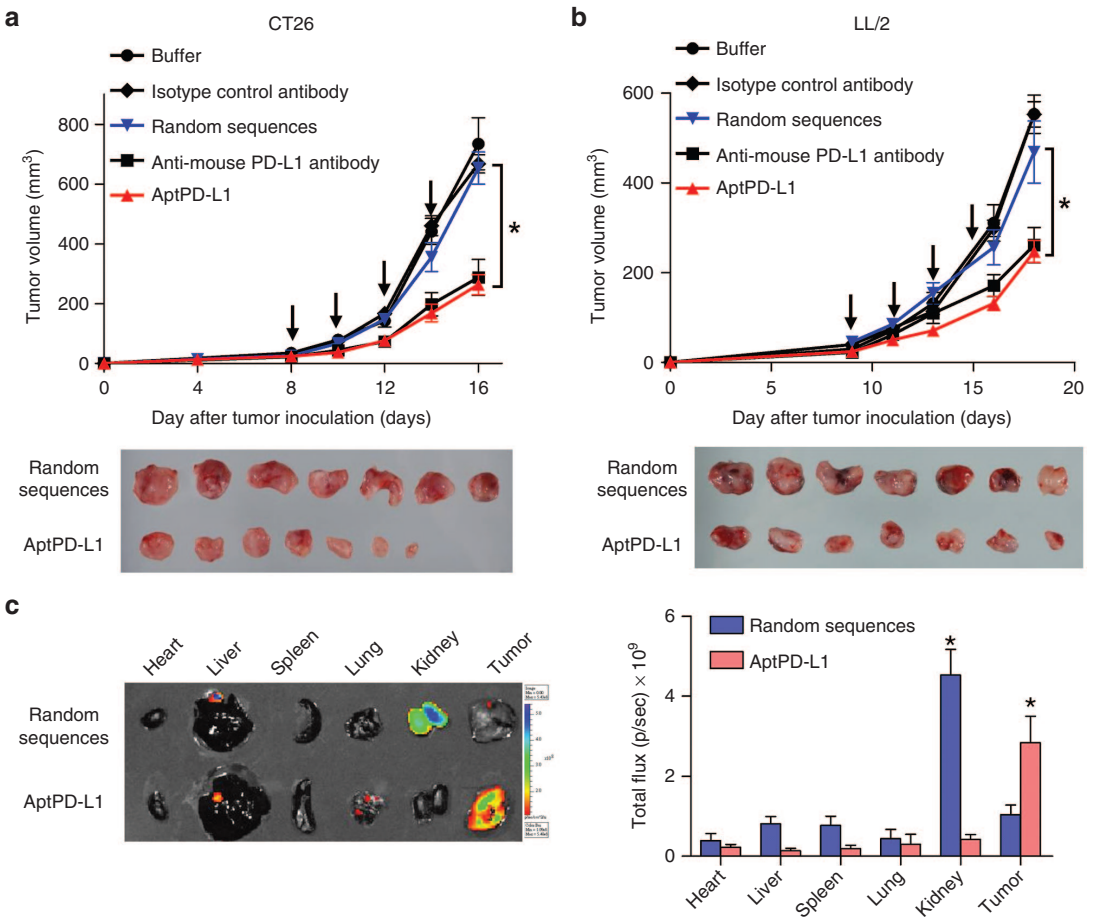

Figure 4 AptPD-L1 accumulates in the PD-L1-expressing tumors and suppresses tumor growth in CT26 colorectal cancer and LL/2 lung cancer murine syngeneic tumor models. (**a, b**) Antibodies (10 mg/kg, $n = 7$ mice/group) or aptamers (1.2 mg/kg, $n = 14$ mice/group) were intraperitoneally administrated on the days indicated by the arrows. (**c**) Biodistribution of random-sequence oligonucleotides or aptPD-L1 (1 μg) 6 hours after intraperitoneally administration ($n = 4$ mice/group). These data are presented as mean ± standard error of the mean and were analyzed by Student's *t*-test. Asterisks denote statistical significant differences ($P < 0.05$).

with optimized length and antagonistic function. Furthermore, docking simulations regarding the interaction between aptamer and PD-L1 added information on removing redundant sequences while preserving the functional structure. This integrated pipeline expedites the development of functional aptamers. The immune checkpoint network is orchestrated by several costimulatory and coinhibitory receptor/ligands. With this integrated pipeline, it is not a formidable task to develop corresponding immune checkpoint targeting therapeutic aptamers.

Materials and methods

Oligonucleotides. All oligonucleotides were synthesized by Integrated DNA Technologies (Coralville, IA). The synthetic ssDNA library used in the SELEX process was composed of 62-nucleotide-long, single-stranded DNAs containing thirty random sequences flanked by the primer sequence, 5'-TCCCTACGGCGCTAAC $[N]_{30}$ GCCACCGTGCTACAAC-3' (where N = A, T, G, or C). The primers used for amplifying ssDNAs were 5'-TCC CTA CGG CGC TAA C-3' (forward) and biotin-labeled 5'-GTT GTA GCA CGG TGG C-3' (reverse). The aptPD-L1 sequence was 5'-ACG GGC CAC ATC AAC TCA TTG ATA GAC AAT GCG TCC ACT GCC CGT-3'.

Cell culture. The human cancer cell lines A549 and HOP92 were cultured in RPMI-1640 medium (Gibco BRL, Life Technologies, Grand Island, NY), and the murine cancer cell lines CT26 and LL/2 were grown in Dulbecco's modified Eagle medium (Gibco BRL). All culture media were supplemented with 10% heat-inactivated fetal bovine serum (Gibco BRL).

Nitrocellulose filter SELEX. The human PD-L1-targeting aptamer was isolated using the nitrocellulose filter SELEX method. In the first round of SELEX, the ssDNA library, comprising 10^{15} molecules, was incubated with 2 μg recombinant human PD-L1 protein (Acrobiosystems, Bethesda, MD) at 37 °C for 30 minutes in SELEX buffer (150 mmol/l NaCl, 5 mmol/l KCl, 1 mmol/l $MgCl_2$, 1 mmol/l $CaCl_2$, and 40 mmol/l HEPES, pH 7.4). ssDNAs bound to PD-L1 protein were then collected on the nitrocellulose filter, and unbound ssDNAs were removed through repetitive washing with SELEX buffer. PD-L1-bound ssDNAs were eluted by heating at 95 °C for 10 minutes and were enriched by PCR. From the second

to the eighth round of SELEX, 10 μg bovine serum albumin was used for negative selection. In brief, eluted ssDNAs that bound to PD-L1 protein were incubated with bovine serum albumin at 37 °C for 30 minutes in SELEX buffer and then passed through a nitrocellulose filter. The flow-through was collected, and ssDNAs were amplified by PCR. After the eighth round of SELEX, PD-L1-bound ssDNAs were subjected to next-generation sequencing on an Illumina MiSeq system (Illumina, San Diego, CA).

Nitrocellulose filter binding assay. Candidate aptamers were incubated with serially diluted recombinant human PD-L1 protein, bovine serum albumin (1.5625, 3.125, 6.25, 12.5, 25, 50, 100, and 200 nmol/l), or mouse PD-L1 protein (6.25, 12.5, 25, 50, 100, 200, and 400 nmol/l) at 37 °C for 30 minutes in SELEX buffer. The aptamer-protein complex was collected by a nitrocellulose filter, and the aptamers were eluted by heating to 95 °C. The number of eluted aptamers was determined by qPCR (ABI PRISM 7900HT; Applied Biosystems, Foster City, CA) using a standard curve constructed using serially diluted candidate aptamers. The K_d of aptPD-L1 for human or mouse PD-L1 recombinant protein was calculated with GraphPad Prism 5 (GraphPad Software, San Diego, CA) using the equation, $Y = A_{max} \times X/(K_d + X)$.

ELISA-based competition assay. Human PD-L1 recombinant protein (2 μg/ml) was coated onto wells of 96-well ELISA plates and blocked with bovine serum albumin (10 mg/ml).

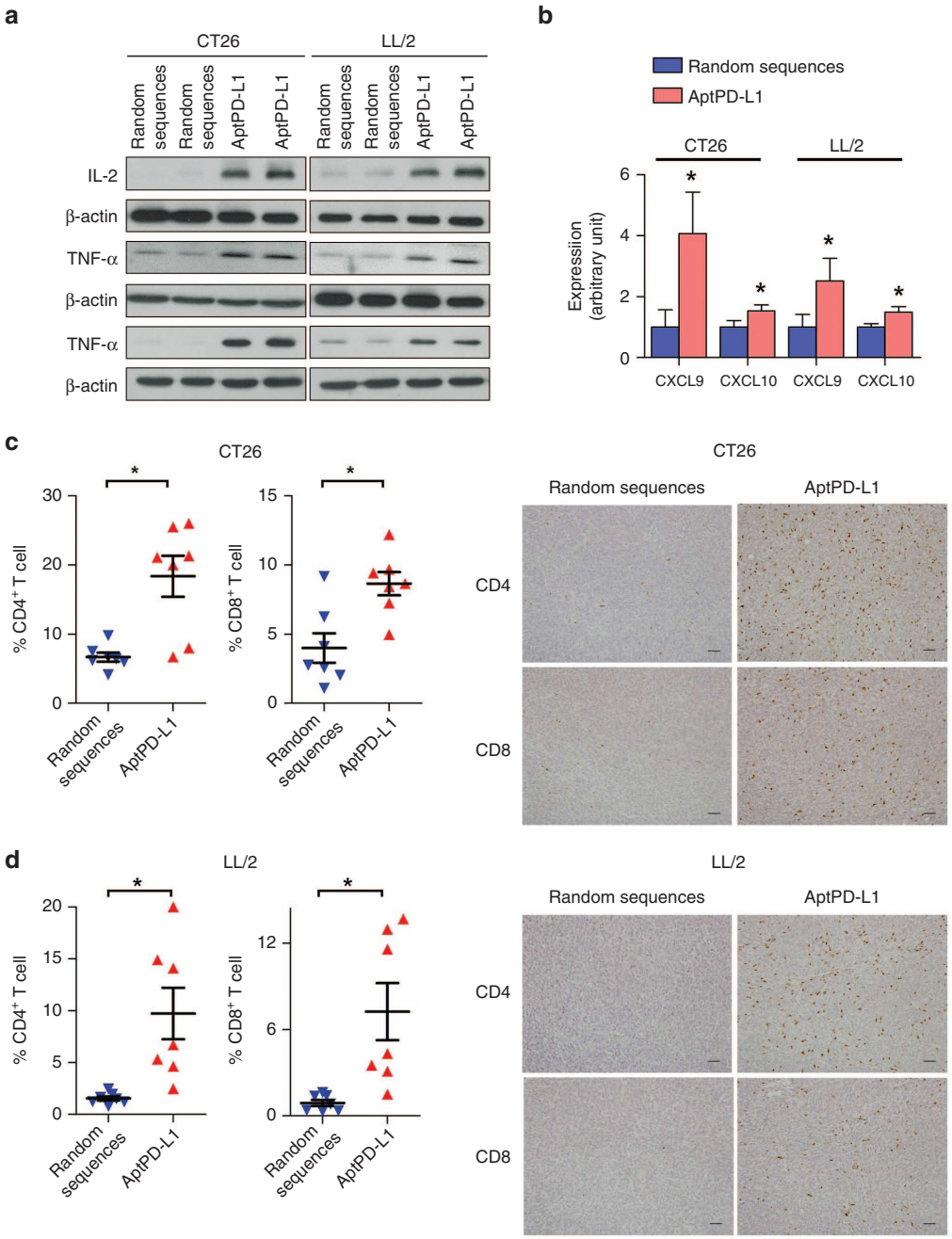

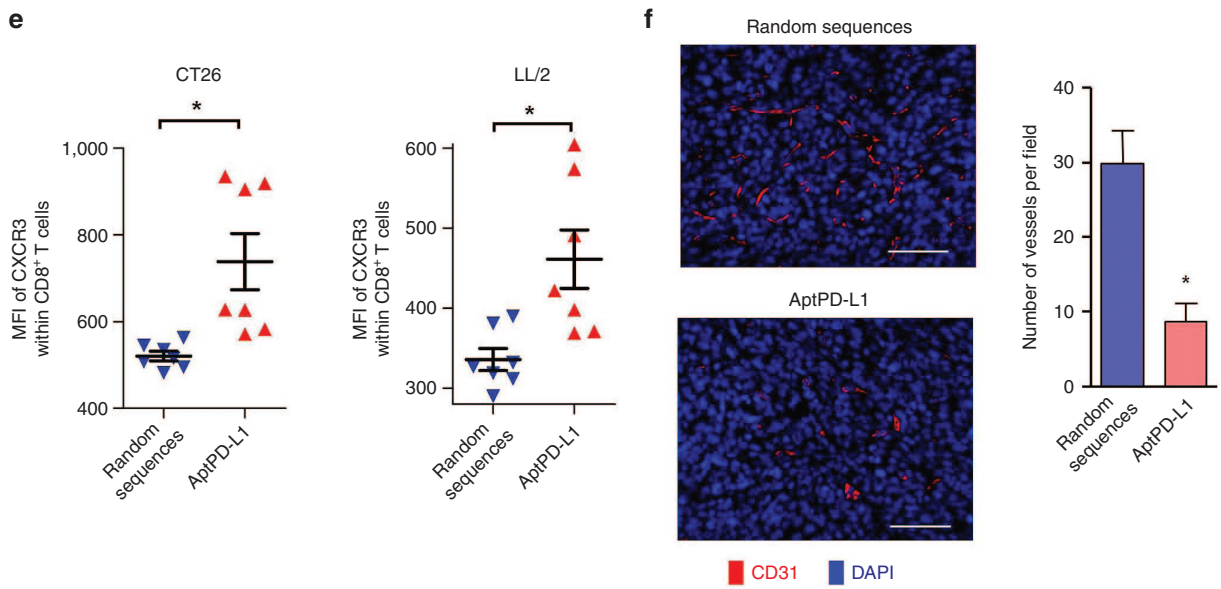

Figure 5 AptPD-L1 significantly induces cytokine expression, augments the number of tumor-infiltrating lymphocytes, and inhibits angiogenesis in tumor tissues. (**a**) IL-2, TNF-α, and IFNγ expression levels were evaluated by immunoblot. β-actin was used as an internal control. (**b**) *CXCL9* and *CXCL10* expression levels were evaluated by quantitative polymerase chain reaction ($n = 7$ mice/group). β-actin was used as an internal control. (**c–e**) Tumor-infiltrating $CD4^+$ and $CD8^+$ T cells and the expression level of CXCR3 were detected by immunohistochemistry staining or flow cytometry ($n = 7$ mice/group). (**f**) Intratumoral vessels were detected using an anti-CD31 antibody in tumors treated with random-sequence oligonucleotides or aptPD-L1 ($n = 7$ mice/group). These data are presented as mean ± standard error of the mean and were analyzed by Student's *t*-test. Asterisks denote statistical significant differences ($P < 0.05$).

Fc-tagged human PD-1 protein (0.6 μg/ml) (Acrobiosystems) and candidate aptamers (200 nmol/l) were simultaneously added into wells. After washing away unbound PD-1 protein, PD-1 that remained in wells was detected by horseradish peroxidase-labeled anti-human IgG antibody (Abcam, Cambridge, UK). 3,3',5,5'-Tetramethylbenzidine (Thermo Scientific, Hudson, NH) was used as an horseradish peroxidase substrate for color development, and absorbance at 652 nm was detected using an ELISA plate reader. The amount of PD-1 protein that remained in the well was quantified by reference to a standard curve constructed using serially diluted human PD-1 protein. Wells without a PD-L1 coating were used as negative controls.

Aptamer structure prediction and aptamer/protein docking simulation. The 2D-structure of aptPD-L1 was predicted using the Mfold web server (http://unafold.rna.albany.edu/?q=mfold/DNA-Folding-Form).[29] Because of the lack of a ssDNA 3D-structure prediction model, we assumed that aptPD-L1 could be modeled as an RNA aptamer and used RNAcomposer (http://rnacomposer.cs.put.poznan.pl/) for 3D-structure prediction.[30] Docking simulations for aptPD-L1 and PD-L1 (PDB 4Z18) proteins were done using the PatchDock Server (http://bioinfo3d.cs.tau.ac.il/PatchDock/).[31,32]

Flow cytometry. Cells were incubated with fluorescence-labeled aptPD-L1 (100 nmol/l, around 1.5 μg/ml) or human PD-L1 antibody (20 μg/ml) (clone 29E.2A3, Biolegend, San Diego, CA) for 30 minutes and then washed twice with SELEX buffer. Random-sequence oligonucleotides or isotype control antibody labeled with fluorescent dye were used as a negative control. Cellular fluorescence intensity was detected using a FACSCalibur flow cytometer (BD Biosciences, San Jose, CA). For dissociation constant determination, serial diluted aptPD-L1 were used and the K_d of aptPD-L1 for PD-L1 protein expressed on cells was calculated using the equation, $Y = B_{max} \times X/(K_d + X)$.

Immunofluorescence staining. Mouse lymphocytes were purified from spleens of BALB/c or C57BL/6 mice (BioLASCO, Taipei, Taiwan) following standard procedures. Lymphocytes were incubated with Alexa Fluor 647-labeled aptPD-L1 in culture medium at 37 °C for 1 hour. After washing with phosphate-buffered saline, lymphocytes were fixed by incubating with 0.25% paraformaldehyde at 4 °C for 30 minutes. Lymphocytes were then immunostained with anti-mouse PD-L1 antibody (D5V3B, Cell Signaling Technology, Beverly, MA) at 4 °C for 1 hour and Alexa Fluor 488-labeled secondary antibodies at 4 °C for 1 hour. Cells were monitored by Axiovert 200 Inverted Fluorescent Microscope (Carl Zeiss, Thornwood, NY). The colocalization of fluorescent signals was analyzed by ImageJ2 software with Coloc 2 plugin and the thresholded Manders split coefficients were calculated.[33,34]

Mouse lymphocyte proliferation assay. Mouse lymphocytes (1×10^5 cells) were labeled with 2 μmol/l Carboxyfluorescein succinimidyl ester (CFSE) (Invitrogen, Carlsbad, CA) at 37 °C for 20 minutes and then cultured in RPMI-1640 supplemented with 10% fetal bovine serum in 96-well plates. Irradiated allogeneic antigen-presenting cells without CFSE labeling (1×10^5 cells) were added into wells and treated with aptamers (200 nmol/l random-sequence oligonucleotides or aptPD-L1). After incubating for 72 hours, lymphocyte

proliferation status was monitored using a FACSCalibur flow cytometer (BD Biosciences). Mouse lymphocytes without CFSE label were used as unstained control. Mouse lymphocytes without cocultured irradiated allogeneic antigen-presenting cells were used as unstimulated control.

Murine syngeneic tumor models. BALB/c mice and C57BL/6 mice were inoculated subcutaneously with CT26 (2×10^5 cells) and LL/2 (1×10^5 cells), respectively. When the long-axis of tumors reached ~5 mm, mice were randomly separated into five groups: (i) buffer, (ii) isotype control antibody (10 mg/kg) (clone RTK4530; BioLegend), (iii) anti-mouse-PD-L1 antibody (10 mg/kg) (clone 10F.9G2; BioLegend), (iv) random-sequence oligonucleotides (1.2 mg/kg), or (v) aptPD-L1 (1.2 mg/kg). Antibodies (n = 7 mice/group) or aptamers (n = 14 mice/group) were administrated intraperitoneally every 2 days. Mice body weight was determined before and after drug administration. According to the guidance of the Laboratory Animal Center, Academia Sinica, when the long-axis of tumors reached ~12 mm, mice blood was collected for blood biochemistry analysis and tumor tissue was collected for flow cytometry analysis, formalin fixation and paraffin embedding, and RNA and protein extraction.

Bio-distribution of aptPD-L1. Alexa Fluor 647-labeled random-sequence oligonucleotides or aptPD-L1 (1μg) were intraperitoneally administrated to mice that bore CT26 tumors. After 6 hours, tissues from heart, liver, spleen, lung, kidney, and tumor were collected and the fluorescent signals emitted from these tissues were detected by Xenogen IVIS Imaging System 200 Series (Caliper Life Sciences, Alameda). The mean of fluorescent signals emitted from buffer-treated group were defined as autofluorescent background signals in the quantification analysis.

Blood biochemistry analysis. The amount of glutamate oxaloacetate transaminase (GOT), glutamic pyruvic transaminase (GPT), and blood urea nitrogen (BUN) were detected by Fuji Dri-Chem 4000i (Fujifilm, Tokyo, Japan) under technical support of Taiwan Mouse Clinic.

Quantitative PCR and western blotting. RNA, extracted from tissues dissected from mice, was purified using a conventional TRIzol (Invitrogen) method following the manufacturer's protocol. cDNA was synthesized from total RNA using oligo$(dT)_{12–18}$ primers and SuperScript III reverse transcriptase (Invitrogen). qPCR was performed on a LightCycler 480 system (Roche Applied Science, Mannheim, Germany) using cDNA as a template and the follow primer pairs (Integrated DNA Technologies): *CXCL9*, 5′-CTT TTC CTC TTG GGC ATC AT-3′ (forward) and 5′-GCA TCG TGC ATT CCT TAT CA-3′ (reverse); *CXCL10*, 5′-GCT GCC GTC ATT TTC TGC-3′ (forward) and 5′-TCT CAC TGG CCC GTC ATC-3′ (reverse); and β-*actin*, 5′-CTA AGG CCA ACC GTG AAA AG-3′ (forward) and 5′-ACC AGA GGC ATA CAG GGA CA-3′ (reverse).

Protein was extracted from tumor tissue using RIPA buffer supplemented with protease inhibitor cocktail (Roche Applied Science). Primary antibodies against the murine proteins IL-2 (Abcam), TNF-α (Abcam), IFNγ (Abcam) were used at a 1:1,000 dilution. Primary antibodies against the murine proteins CXCL9 and CXCL10 (R&D Systems, Minneapolis, MN) were used at a 1:500 dilution. The primary antibody against β-actin (Santa Cruz Biotechnology, Santa Cruz, CA) was used at 1:10,000 dilution. horseradish peroxidase-labeled secondary antibodies were used at a 1:5,000 dilution (Santa Cruz Biotechnology).

Flow cytometry analysis and immunohistochemical staining of tumors. Tumors were digested with collagenase and cells in the tumors were isolated following the procedures built by Zabel *et al.*[35] Antibodies against mouse CD45, CD4, CD8, CXCR3, or relative isotype control antibodies (BioLegend) were used to stain these isolated cells. $CD45^+$ cells were gated and the leukocyte subsets were further analyzed by other CD markers. Formalin-fixed, paraffin-embedded tissues were rehydrated and subjected to an antigen-retrieval process in citrate buffer (pH 6.0). Primary antibodies against mouse CD4 (Thermo Scientific) or CD8 (Thermo Scientific) were used at a 1:100 dilution and counterstained with hematoxylin. For immunofluorescence staining, primary antibodies against CD31 (Abcam) were used at a 1:100 dilution. Alexa Fluor 647-labeled secondary antibodies (Abcam) were used at a 1:500 dilution. Nuclei were stained with DAPI in Fluoroshield mounting medium (Abcam).

Statistical analysis. All data in bar graphs are presented as means ± standard error of the mean and were analyzed using a two-sided Student's *t*-test. *P* values < 0.05 were considered statistically significant.

Acknowledgments This work was supported by Academia Sinica (grant number 2399-1040101). The authors thank Dr. Kuo-I Lin for technical support with experiments related to lymphocyte proliferation assays. We also thank the National Center for Genome Medicine for NGS technical and bioinformatics support. The authors report no conflicts of interest.

Supplementary material

Table S1. Summary of the NGS sequencing data.
Table S2. AptPD-L1 treatment does not induce observable liver or renal toxicity.
Figure S1. AptPD-L1 blocks PD-L1/PD-1 interactions.
Figure S2. AptPD-L1 binds to PD-L1-expressing murine cancer cells.
Figure S3. AptPD-L1 has no direct cytotoxic effect against murine cancer cells.
Figure S4. AptPD-L1 does not affect mice body weight.
Figure S5. AptPD-L1 significantly induces cytokine expression in tumor tissues.

1. Sharma, P and Allison, JP (2015). Immune checkpoint targeting in cancer therapy: toward combination strategies with curative potential. *Cell* **161**: 205–214.
2. Domling, A and Holak, TA (2014). Programmed death-1: therapeutic success after more than 100 years of cancer immunotherapy. *Angew Chem Int Ed* **53**: 2286–2288.
3. Smyth, MJ, Ngiow, SF, Ribas, A and Teng, MW (2016). Combination cancer immunotherapies tailored to the tumour microenvironment. *Nat Rev Clin Oncol* **13**: 143–158.

4. Okazaki, T, Chikuma, S, Iwai, Y, Fagarasan, S and Honjo, T (2013). A rheostat for immune responses: the unique properties of PD-1 and their advantages for clinical application. *Nat Immunol* **14**: 1212–1218.
5. Herbst, RS, Soria, JC, Kowanetz, M, Fine, GD, Hamid, O, Gordon, MS *et al.* (2014). Predictive correlates of response to the anti-PD-L1 antibody MPDL3280A in cancer patients. *Nature* **515**: 563–567.
6. Okazaki, T and Honjo, T (2007). PD-1 and PD-1 ligands: from discovery to clinical application. *Int Immunol* **19**: 813–824.
7. Callahan, MK and Wolchok, JD (2013). At the bedside: CTLA-4- and PD-1-blocking antibodies in cancer immunotherapy. *J Leukoc Biol* **94**: 41–53.
8. Intlekofer, AM and Thompson, CB (2013). At the bench: preclinical rationale for CTLA-4 and PD-1 blockade as cancer immunotherapy. *J Leukoc Biol* **94**: 25–39.
9. Samaranayake, H, Wirth, T, Schenkwein, D, Räty, JK and Ylä-Herttuala, S (2009). Challenges in monoclonal antibody-based therapies. *Ann Med* **41**: 322–331.
10. Prodeus, A, Abdul-Wahid, A, Fischer, NW, Huang, EH, Cydzik, M and Gariépy, J (2015). Targeting the PD-1/PD-L1 immune evasion axis with DNA aptamers as a novel therapeutic strategy for the treatment of disseminated cancers. *Mol Ther Nucleic Acids* **4**: e237.
11. Mayer, G (2009). The chemical biology of aptamers. *Angew Chem Int Ed* **48**: 2672–2689.
12. Lao, YH, Phua, KK and Leong, KW (2015). Aptamer nanomedicine for cancer therapeutics: barriers and potential for translation. *ACS Nano* **9**: 2235–2254.
13. Sun, H, Zhu, X, Lu, PY, Rosato, RR, Tan, W and Zu, Y (2014). Oligonucleotide aptamers: new tools for targeted cancer therapy. *Mol Ther Nucleic Acids* **3**: e182.
14. Dollins, CM, Nair, S and Sullenger, BA (2008). Aptamers in immunotherapy. *Hum Gene Ther* **19**: 443–450.
15. Gilboa, E, McNamara, J 2nd and Pastor, F (2013). Use of oligonucleotide aptamer ligands to modulate the function of immune receptors. *Clin Cancer Res* **19**: 1054–1062.
16. Xiang, D, Shigdar, S, Qiao, G, Wang, T, Kouzani, AZ, Zhou, SF *et al.* (2015). Nucleic acid aptamer-guided cancer therapeutics and diagnostics: the next generation of cancer medicine. *Theranostics* **5**: 23–42.
17. Ng, EW, Shima, DT, Calias, P, Cunningham, ET Jr, Guyer, DR and Adamis, AP (2006). Pegaptanib, a targeted anti-VEGF aptamer for ocular vascular disease. *Nat Rev Drug Discov* **5**: 123–132.
18. Kato, K, Ikeda, H, Miyakawa, S, Futakawa, S, Nonaka, Y, Fujiwara, M *et al.* (2016). Structural basis for specific inhibition of Autotaxin by a DNA aptamer. *Nat Struct Mol Biol* **23**: 395–401.
19. Chen, L, Li, DQ, Zhong, J, Wu, XL, Chen, Q, Peng, H *et al.* (2011). IL-17RA aptamer-mediated repression of IL-6 inhibits synovium inflammation in a murine model of osteoarthritis. *Osteoarthritis Cartilage* **19**: 711–718.
20. Wheeler, LA, Trifonova, R, Vrbanac, V, Basar, E, McKernan, S, Xu, Z *et al.* (2011). Inhibition of HIV transmission in human cervicovaginal explants and humanized mice using CD4 aptamer-siRNA chimeras. *J Clin Invest* **121**: 2401–2412.
21. Ozer, A, Pagano, JM and Lis, JT (2014). New technologies provide quantum changes in the scale, speed, and success of SELEX methods and aptamer characterization. *Mol Ther Nucleic Acids* **3**: e183.
22. Blind, M, and Blank, M (2015). Aptamer selection technology and recent advances. *Mol Ther Nucleic Acids* **4**: e223.
23. Alam, KK, Chang, JL and Burke, DH (2015). FASTAptamer: a bioinformatic toolkit for high-throughput sequence analysis of combinatorial selections. *Mol Ther Nucleic Acids* **4**: e230.
24. Li, W, Cowley, A, Uludag, M, Gur, T, McWilliam, H, Squizzato, S *et al.* (2015). The EMBL-EBI bioinformatics web and programmatic tools framework. *Nucleic Acids Res* **43**(W1): W580–W584.
25. Lin, DY, Tanaka, Y, Iwasaki, M, Gittis, AG, Su, HP, Mikami, B *et al.* (2008). The PD-1/PD-L1 complex resembles the antigen-binding Fv domains of antibodies and T cell receptors. *Proc Natl Acad Sci USA* **105**: 3011–3016.
26. Chow, MT and Luster, AD (2014). Chemokines in cancer. *Cancer Immunol Res* **2**: 1125–1131.
27. Groom, JR and Luster, AD (2011). CXCR3 in T cell function. *Exp Cell Res* **317**: 620–631.
28. Singh, S, Sadanandam, A and Singh, RK (2007). Chemokines in tumor angiogenesis and metastasis. *Cancer Metastasis Rev* **26**: 453–467.
29. Zuker, M (2003). Mfold web server for nucleic acid folding and hybridization prediction. *Nucleic Acids Res* **31**: 3406–3415.
30. Popenda, M, Szachniuk, M, Antczak, M, Purzycka, KJ, Lukasiak, P, Bartol, N *et al.* (2012). Automated 3D structure composition for large RNAs. *Nucleic Acids Res* **40**: e112.
31. Duhovny, D, Nussinov, R and Wolfson, HJ (2002). Efficient unbound docking of rigid molecules. *Lect Notes Comput Sc* **2452**: 185–200.
32. Schneidman-Duhovny, D, Inbar, Y, Nussinov, R and Wolfson, HJ (2005). PatchDock and SymmDock: servers for rigid and symmetric docking. *Nucleic Acids Res* **33**(Web Server issue): W363–W367.
33. Schindelin, J, Rueden, CT, Hiner, MC and Eliceiri, KW (2015). The ImageJ ecosystem: an open platform for biomedical image analysis. *Mol Reprod Dev* **82**: 518–529.
34. Schindelin, J, Arganda-Carreras, I, Frise, E, Kaynig, V, Longair, M, Pietzsch, T *et al.* (2012). Fiji: an open-source platform for biological-image analysis. *Nat Methods* **9**: 676–682.
35. Pachynski, RK, Scholz, A, Monnier, J, Butcher, EC and Zabel, BA (2015). Evaluation of tumor-infiltrating leukocyte subsets in a subcutaneous tumor model. *J Vis Exp* **98**: e52657.

Supplementary Information accompanies this paper on the Molecular Therapy–Nucleic Acids website (http://www.nature.com/mtna)